Design, implementation and speed estimation of three-phase 2 kW out-runner permanent magnet BLDC motor for ultralight electric vehicles

Article *in* Electrical Engineering · October 2021

DOI: 10.1007/s00202-021-01279-5

1 author:

Alper Kerem
Kahramanmaras Sutcu Imam University
33 PUBLICATIONS **165** CITATIONS

SEE PROFILE

Electrical Engineering (2021) 103:2547–2559
https://doi.org/10.1007/s00202-021-01279-5

ORIGINAL PAPER

Design, implementation and speed estimation of three-phase 2 kW out-runner permanent magnet BLDC motor for ultralight electric vehicles

Alper Kerem[1]

Received: 7 January 2021 / Accepted: 24 March 2021 / Published online: 10 April 2021

Abstract
Brushless DC motor has specifications such as high efficiency, high startup moment and silent running. Thanks to its low inertia, high torque/size and power/size ratio, it can be used in specially designed vehicles such as electric vehicles (EVs), spacecraft and submarines. As there is no brush and commutator that in its structure can cause arc forming, it can be used in fire-sensitive areas. In this study, a 2 kW three-phase out-runner permanent magnet brushless DC (BLDC) motor was designed to be used in ultralight EV. The size of the motor, the magnetic equivalent circuit and the electrical equivalent circuit parameters required for the BLDC motor design process were analytically calculated. The finite element method was then used to evaluate flux density, flux distributions, torque and motor efficiency and was approved for analytical design. The BLDC motor, which has about 89% efficiency, has been manufactured and mounted on an ultralight EV. Finally, the motor speed was estimated using a new robust hybrid metaheuristic model called artificial neural networks (ANNs) trained with particle swarm optimization (PSO) and radial movement optimization (RMO). A genuine and unconventional technique was used to examine the model's performance. That is, using three distinct input variables such as output torque, efficiency and output power, the output variable of motor speed was estimated. And then, the results were compared using the other three hybrid models. In all performs, it was seen that ANNs trained with PSO + RMO model achieved the most successful results with the lowest errors.

Keywords Permanent magnet BLDC · Ultralight electric vehicle · In-wheel electric motor · Finite element method (FEM) · Metaheuristic algorithm

1 Introduction

Fossil-based energy sources are considered limited in nature and will be consumed over time. However, there are still many sectors dependent on this energy resource which will be depleted. A significant position in this field is occupied by the increasingly growing number of internal combustion engine automobiles. An effective alternative that can reduce this dependency is electric vehicles (EVs).

EVs compose of three main components such as the battery, the electric motor and the electricity transmission system [1]. There are two types of electric motors used in EVs: an inner rotor and an outer rotor. In models that use internal rotor motors, mechanical differentials and gears are widely used. On the other hand, outer-rotor motors do not require additional mechanical components, since they are normally mounted inside the wheels. As its power used in these models is transferred directly to the wheels, compared to the inner rotor model, higher efficiency can be achieved [2].

In literature for BLDC motor designs, Apatya et. Al. [3] designed and produced a BLDC motor with a three-phase internal rotor, 8-pole and 12-slot. They also demonstrated that the material quality is quite effective in terms of motor efficiency. Shrivastava and Brahmin [4] designed 15 kW and three-phase double layer coil BLDC motor for EVs with 94.3% efficiency. Jurkovic and Žarko [5] optimized the low mass permanent magnet BLDC motor for the propulsion of an ultralight aircraft. The aim

✉ Alper Kerem
alperkerem@ksu.edu.tr

[1] Electrical Electronics Engineering Department, Kahramanmaraş Sütçü İmam University, 46100 Kahramanmaraş, Turkey

of the optimization is to have a nominal power of 15 kW at a nominal speed of 3000 rpm at a hot-spot temperature not reaching the temperature limits of Class F insulation (155 °C). Bogusz et. al [6] designed an 800 W BLDC motor for unmanned aerial vehicles. And, it has demonstrated how the shape and magnetizing technique affect the cogging torque and average torque of the motor. Castano and Maixé [7] designed a new BLDC motor to power fan of the automobile air conditioning system. Compared to the existing commercial BLDC motor, they achieved 5% better performance. Mukherjee and Sengupta [8] designed 560 W BLDC motor with 87% efficiency. Gholase and Fernandes [9] designed a low-cost and powerful ferrite magnet-based BLDC motor to provide an alternative to the universal motor in a mixer-grinder. Bogusz et al. [10] designed three-phase BLDC motor with permanent magnet using in hybrid drive for a small unmanned aerial vehicle. While using 0.35-mm thick non-oriented magnetic steel sheets, the average performance of the developed drive system at a speed of 8000 rpm with 87.3% efficiency. Khergade et al. [11] designed a slotless axial flux permanent magnet (AFPM) BLDC motor for EVs thanks form which is versatility, compactness, robustness, high performance, large speed range and high torque. He and Wu [12] aimed to design the most appropriate BLDC motor for the electric impact wrench that meets all industry requirements, thus designing a 400 W motor. Jafarboland and Farahabadi [13] optimally configured the stator parameters in the BLDC motor to eliminate noise and vibration. Compared to the prototype one, they managed to reduce the total average amplitude of vibration displacements in the stator by 75.4% at the end of the optimizing trials. Tutelea and Boldea [14] developed a 200 W BLDC motor for home appliances with finite element method (FEM) validation using the Hooke Jeeves method. Nair et al. [15] desingned an axial field permanent magnet (AFBLDC) motor for automotive applications. By shaping the slots and magnets, FEA helped to refine the structure, and thus, the back-emf waveform was strengthened and cogging torque was decreased. Park et al. [16] developed an outer-rotor BLDC motor with a halbach magnet array to increase the power structure of BLDC for drones. Shahri et al. [17] aimed to increase the performance and decrease the torque ripple frequency of BLDC motor by adjusting the dimensions of the stator sluts using adaptive multi-objective optimization. Singh et al. [18] developed and analyzed the permanent magnet BLDC motor for using in hybrid EVs/ solar vehicles. Literature for three-phase BLDC motor designs is shown in Table 1.

A three-phase, 2 kW, 830 rpm and 89% efficiency outrunner permanent magnet BLDC motor was analytically designed in this study. The success of analytical design has been confirmed by analyzing of torque, speed and motor efficiencies, especially flux density and flux distributions with using FEM. After FEM-based validation process, the BLDC motor was produced and mounted on an ultralight EV. The speed estimation studies of BLDC motor using a new robust hybrid metaheuristic model named ANNs trained with PSO + RMO were carried out. Its performance comparisons with other hybrids such as ANNs trained with particle swarm optimization (PSO), ANNs trained with genetic algorithm (GA) and ANNs trained with ant colony optimization

Table 1 Literature for three-phase BLDC motor designs

Rotor type	Slot/pole	Rated power	Rated voltage	Rated speed (rpm)	Rated torque	Efficiency	References
Inner	12/8	–	–	300	–	–	[3]
Outer	36/24	15,000 W	300 V	1070	135 Nm	94.3%	[4]
Inner	12/10 18/16	15,000 W	100 V	3000	47.5 Nm	–	[5]
Outer	12/14	800 W	27 V	8000	–	85%	[6]
Inner	12/4	92.88 W	24 V	1800	0.3 Nm	62.83%	[7]
Inner	24/4	560 W	400 V	1500	0.706 Nm	87%	[8]
Inner	9/6	200 W	48 V	10,000	0.19 Nm	> 80%	[9]
Outer	24/20	800 W	52 V	8000	–	87.3%	[10]
Outer	24/36	–	48 V	1000	0.34 Nm	–	[11]
Inner	6/4	400 W	20 V	18,000	0.014 Nm	–	[12]
Inner	12/10	349 W	60 V	7600	0.44 Nm	88.32%	[13]
Inner	6/4	200 W	300 V	1500	0.02 Nm–1.5 Nm	94.04%	[14]
Axial	24/8	4500 W	48 V	2500	17 Nm	–	[15]
Outer	12/14	19.6 W	6.2 V	5500	0.035 Nm	83.7%	[16]
Outer	12/14	110 W	13.5 V	3000	0.35 Nm	88%	[17]
Inner	12/4	1500 W	100 V	3000	5.107 Nm	94.06%	[18]

(ACO) were presented in tables. The graphic and figures of the designed three-phase in-whell out-runner permanent magnet BLDC motor are shown in the next sections.

2 Out-runner permanent magnet BLDC motor design

In the industry, especially in the automotive sector, BLDC motors are commonly used thanks to their simple design, high resistance, run at high speed ability [3, 19], high torque [5], high efficiency [11], small size, light weight [20], simple installation and cooling [21] and high power density. However, permanent magnet BLDC motors are exposed to cogging torque that causes vibration and noise in shaft. This is undesirable in terms of motor performance and studies are continuing to reduce cogging torque [22].

As not every motor is appropriate per each project, it is necessary to determine the aim of the motor's usage before the design begins. Then, to design and to produce the most appropriate motor, type of magnetic material, motor dimensions, air gap, winding configuration, magnet selection, slot-fractional selections, etc., must be carefully determined [3, 20]. In addition, during construction practice, ambient/operating temperature and space restrictions should be taken into consideration. The flowchart of the designed out-runner permanent magnet BLDC motor is given in Fig. 1.

As shown in Fig. 1, firstly, the design specifications were determined such as rated power, rated speed, rated moment, rated voltage, efficiency and operating frequency. Secondly, the number of slots, number of poles, magnet material and rotor configurations were examined. Thirdly, with some practice, diameter of stator, diameter of rotor and air gap were determined. And then, the processes of rotor configuration, length of air gap and windings were determined meticulously. All of these stages are optimized to obtain better efficiency and adequate torque at low and high speeds from the BLDC motor.

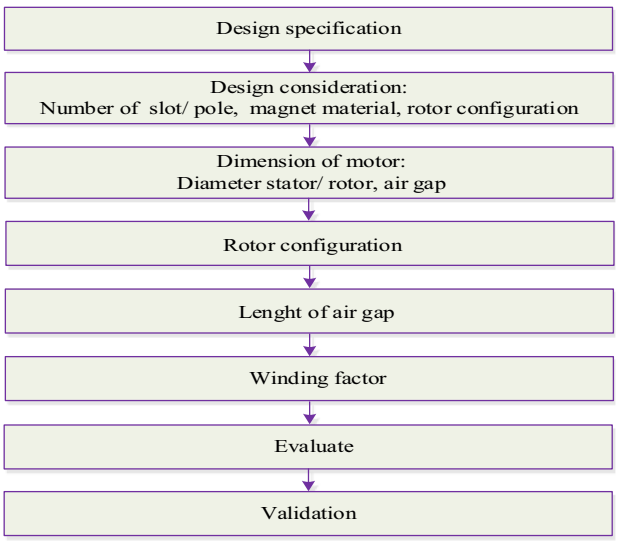

Fig. 1 Flowchart of the designed out-runner permanent magnet BLDC motor [3]

2.1 Main dimensions

It is critical to identify the rated power (P_{out}), rated speed (ω), desired efficiency (η) and rated torque (T_e) parameters when beginning the design process. And, with a good engineering endeavor number of phases, number of slots (Q_s) and number of poles (p) can be determined. In contrast to a single or two phase winding, a three-phase stator winding provides better copper usage and lower torque ripple. For low and medium voltage BLDC motors, increasing the number of phases to four or five is not advised, as the cost of both the copper winding and the drive system switching components would rise considerably [23]. Initial parameters of out-runner permanent magnet BLDC motor are shown in Table 2.

2.2 Mechanical parameters

For the realization of output equations and performance formulas in the motor sizing process, motor length and stator-rotor diameter sizes are significant. Other dimensions within the scope of winding studies can be obtained by performance-based parametric solutions. Geometric parameters for outer-rotor BLDC motor are shown in Fig. 2.

Where r_{out} is motor's outer radius, r_δ is airgap radius in mm, h_m is permanent magnets height and h_{ry} is the rotor yoke height defined by Eq. (1). b_{st} is the slow teeth width, δ is the airgap length, h_{sw} is the stator tooth tip height, Q_s is the stator slot number and b_{ss1} is the slot top width defined by Eq. (2). b_{ss2} is the slot base width and h_{ss} is the stator slot

Table 2 Initial design parameters

Parameters	Values	Units
Rated power	2	kW
Maximum output power	2.5	kW
Rated speed	700–900	rpm
Rated moment	23–25	Nm
Rated voltage	96	V
Maximum efficiency	90%	–
Frequency	50	Hz
Stator material	M330-50A	–
Rotor material	AISI/SAE 4340 alloy steel	–
Magnet type	N40UH	–

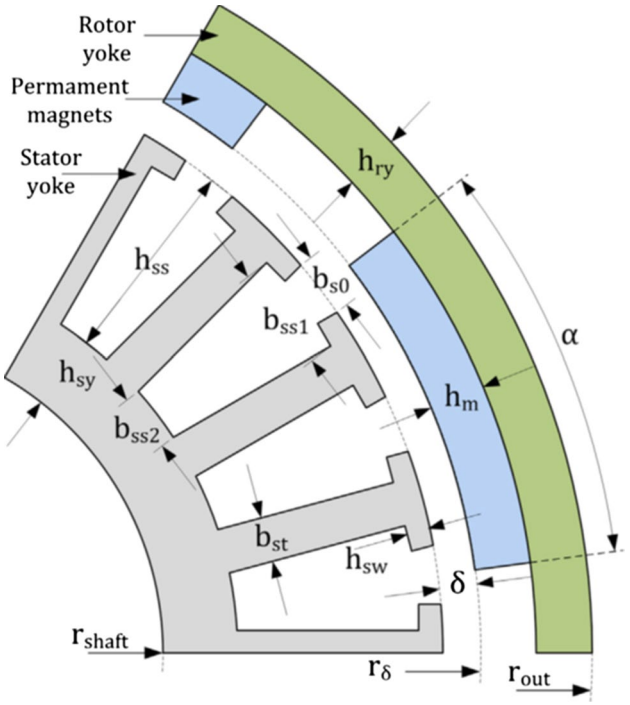

Fig. 2 Geometric parameters of outer-rotor BLDC motor [23]

Table 3 Geometric parameters for BLDC motor

Prmtr	Definition	Description	Equations
r_{out}	$r_{out} = r_\delta + \delta + h_m + h_{ry}$	Motor's outer radius	(1)
b_{st}	$b_{st} = \frac{2\pi(r_\delta - \delta - h_{sw})}{Q_s} - b_{ss1}$	Slow teeth width	(2)
b_{ss2}	$b_{ss2} = \frac{2\pi(r_\delta - \delta - h_{ss})}{Q_s} - b_{st}$	Slot base width	(3)
h_{sy}	$h_{sy} = r_\delta + \delta - r_{shaft} - h_{ss}$	Stator yoke height	(4)
h_{ss}	$h_{ss} = (r_\delta + \delta - r_{shaft}) - \frac{\pi B_m}{pB_{sy}}$	Stator slot height	(5)
A_{slot}	$A_{slot} = \frac{1}{2}(b_{ss1} + b_{ss2})(h_{ss} - h_{sw})$	Total slot area	(6)
k_{open}	$k_{open} = \frac{b_{s0}}{b_{ss1}}$	Ratio of stator slot opening to slot width	(7)

height defined by Eq. (3). h_{sy} is the stator yoke height and r_{shaft} is the motor shaft radius defined by Eq. (4). B_m is the fundamental airgap flux density and B_{sy} is the flux density at stator yoke defined by Eq. (5). A_{slot} is the total slot area defined by Eq. (6). k_{open} is the ratio of stator slot opening to slot width and b_{s0} is the Carter's coefficient slot opening width defined by Eq. (7) in Table 3 [23].

2.3 Electrical and magnetic parameters

The height of permanent magnets (h_m) and the pole arc to pole pitch ratio (α) are of considerable significance, since they basically affect the density of airgap flux and the efficiency of the motor [23] (Table 4).where B_m is the fundamental airgap flux density, B_r is the remnant flux density of the magnet, leakage factor representing the percentage of the flux lines that pass through the airgap is k_{leak}, μ_r shows relative magnet permeability, δ is the airgap length, h_m is the height of permanent magnets, k_c is the Carter factor defined by Eq. (8). Constant c is considered equal to 3.0 for an outer-rotor topology defined by Eq. (9). τ_s is the slot pitch defined by Eqs. (10) and Eq. (11). φ_{pole} is the magnetic flux of each pole, A_{pole} is the pole's area, L is the motor's axial length defined by Eq. (12). φ_{sy} is the magnetic flux at stator and φ_{ry} is the magnetic flux at rotor defined by Eq. (13). B_{sy} is the flux density at stator yoke and B_{ry} is the flux density at rotor yoke for Eqs. (14) and (15), respectively [23]. Electrical parameters for BLDC motor are shown in Table 5.where N_{ph} is the number of turns per phase, E_{ph} is the produced back-emf and ω is the rated angular speed defined by Eq. (16). J_{Cu} is the copper wire's current density and s_{ff} is the stator slot fill factor defined by Eq. (17). I_{rms} is the rms phase current defined by Eq. (18). I_{DC} is the DC-link current defined by Eq. (19). T_e is the produced torque, V_{DC} is the DC-link voltage, K_{Eph} is the back-emf constant, Rc is the internal resistance of coil winding defined by Eq. (20). η is the efficiency, P_{cu} is the copper losses, P_{eddy} is the eddy current losses, P_{hyst} is the hysteresis losses and P_{fric} is the frictional losses defined by Eq. (21) [23, 24]. Analytical calculation results of out-runner BLDC motor are shown in Table 6.

3 FEM-based validation

FEM is being used to solve electromagnetic field issues, by using Poisson's type variational calculus from simple magnetostatic Maxwell equations. The complicated internal structure and nonlinear materials present in the machine structure can be managed by it [21]. It is a supplement to circuit approach used to analyze the parameters of motor design, which has a short computation time; however, its accuracy is limited by the motor design concept [25]. The flux density, flux distribution, flux path and the mesh in BLDC motor can be analyzed using FEM [24].

Newly designed three-phase out-runner permanent magnet BLDC motor was simulated by using Ansoft Maxwell 3D electromagnetic simulation FEM software. Figure 3 illustrates the magnetic flux distribution of designed BLDC motor.

Figure 3 illustrates the presence of saturation in the stator circuit. The material used in the stator is M330-50A and,

Table 4 Magnetic parameters for BLDC motor

Prmtr	Definition	Description	Equations
B_m	$B_m = \frac{B_r k_{\text{leak}}}{1+\frac{\mu_r \delta k_c}{h_m}}$	Airgap flux density	(8)
k_{leak}	$k_{\text{leak}} = \frac{100-(\frac{7p}{60}-c)}{100}$	Leakage factor	(9)
k_c	$k_c = \tau_s\left(\tau_s - \frac{(k_{\text{open}} b_{ss1})^2}{(k_{\text{open}} b_{ss1}+5\delta)}\right)^{-1}$	Carter factor	(10)
t_s	$\tau_s = \pi \frac{D_\delta}{Q_s}$	Slot pitch	(11)
φ_{pole}	$\varphi_{\text{pole}} = B_m A_{\text{pole}}$ and $A_{\text{pole}} = \frac{\pi D_\delta L}{p}$	Magnetic flux of each pole	(12)
φ_{sy}	$\varphi_{\text{sy}} = \varphi_{\text{ry}} = \frac{\varphi_{\text{pole}}}{2}$	Magnetic flux at stator/rotor yoke	(13)
B_{sy}	$B_{\text{sy}} = \frac{\varphi_{\text{sy}}}{h_{\text{sy}} L}$	Flux density at stator yoke	(14)
B_{ry}	$B_{\text{ry}} = \frac{\varphi_{\text{ry}}}{h_{\text{ry}} L}$	Flux density at rotor yoke	(15)

Table 5 Electrical parameters for BLDC motor

Pr	Definition	Descript	Equations
N_{ph}	$N_{\text{ph}} = \frac{E_{\text{ph}}}{2B_m L(r_\delta-\delta)\omega}$	Number of turns per phase	(16)
J_{Cu}	$J_{\text{Cu}} = \frac{2\pi q(r_\delta-\delta)}{s_{ff} A_{\text{slot}}}$	Copper wire's current density	(17)
I_{rms}	$I_{\text{rms}} = \frac{2\pi q(r_\delta-\delta)}{6N_{ph}}$	Rms phase current	(18)
I_{DC}	$I_{\text{DC}} = \sqrt{\frac{3}{2}} I_{\text{rms}}$	DC-link current	(19)
T_e	$T_e = \frac{K_t(V_{\text{DC}}-K_{\text{Eph}}\omega)}{2R_c}$	Produced torque	(20)
η	$\eta = \frac{T_e\omega}{T_e\omega+P_{\text{Cu}}+P_{\text{eddy}}+P_{\text{hyst}}+P_{\text{fric}}}$	Motor efficiency	(21)

Table 6 Analytical calculation results of out-runner BLDC motor

Parameters	Values	Units
Rated power	2	kW
Rated speed at 50 Hz	830	rpm
Operating voltage	96	V
Efficiency	~%90	–
Rated torque	23	Nm
Slot/pole	36/40	–
Stator inner diameter	194	mm
Rotor outer diameter	273	mm
Stack length	25	mm
Type of operating	Direct drive	–
Rotor type	Nickel coated N40UH type neodymium permanent magnets	–
Magnet temp	180	°C
Ball bearing type	SKF/FAG ring	–
Total weight of stator and rotor	~10.4	kg

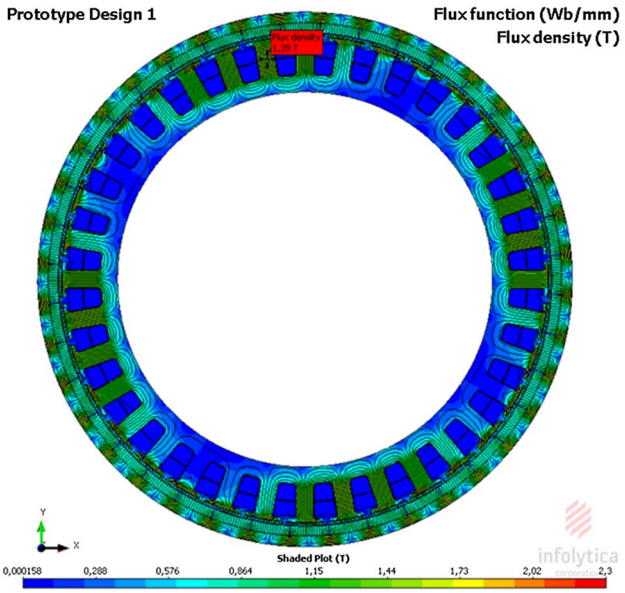

Fig. 3 Flux distribution of designed out-runner permanent magnet BLDC motor

considering the saturation value, it was carefully selected. As seen in Fig. 3, the flux density value of the designed motor is 1.39 T, and it is quite efficient. The flux drain regions will turn light green to yellow as the Tesla value approaches at 2. Additionally, this color would transform from orange to red when the motor is saturated. This BLDC motor, however, has been designed meticulously so that it can drain the flux without causing oversaturation. The ¼ flux distribution and flux pattern of designed out-runner permanent magnet BLDC motor are given in Figs. 4 and 5, respectively.

Figure 6 shows the relationship between rms current and speed. Due to the structural characteristics of the motor, it draws excessive current at initial moment. This excessive current value drawn decrease depending on the time. As can be seen from Fig. 6, the current drawn by the designed

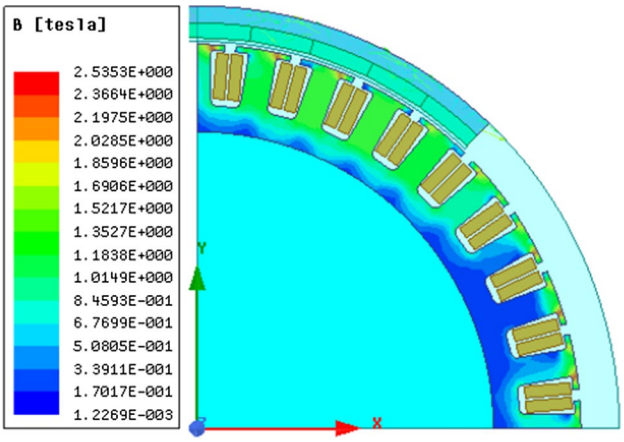

Fig. 4 ¼ flux distribution of the designed out-runner permanent magnet BLDC motor

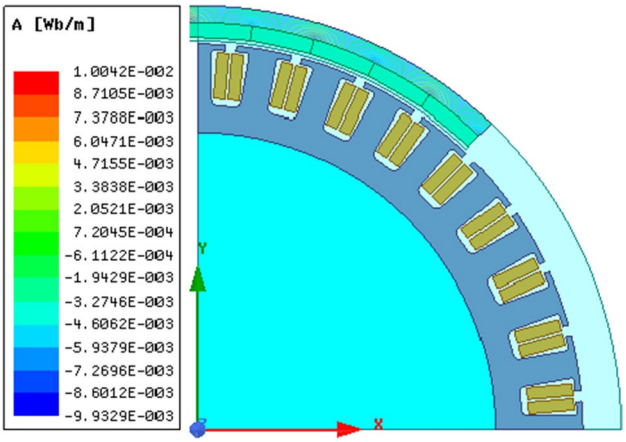

Fig. 5 ¼ flux pattern of the designed out-runner permanent magnet BLDC motor

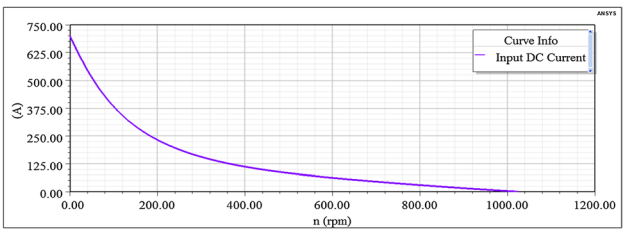

Fig. 6 Rms current versus speed

BLDC motor decreased rapidly depending on the time. It draws so little current at its rated speed of 830 rpm.

Figure 7 shows the relationship between efficiency and speed. The rated speed was accepted as 700–900 rpm in the initial design study. After the optimization process, it determined 830 rpm, which was the most effective rpm value.

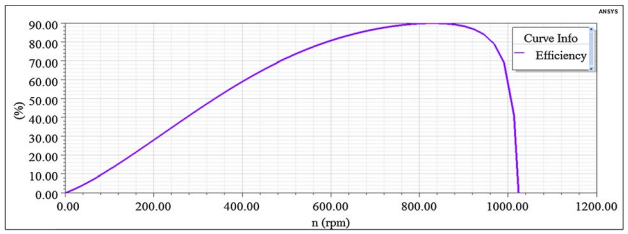

Fig. 7 Efficiency versus speed

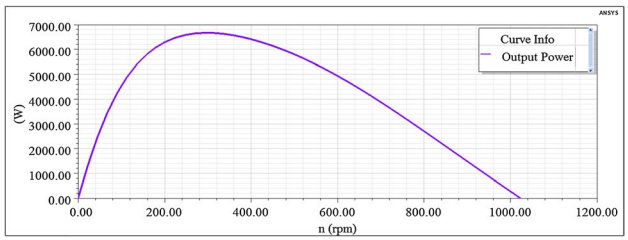

Fig. 8 Output power versus speed

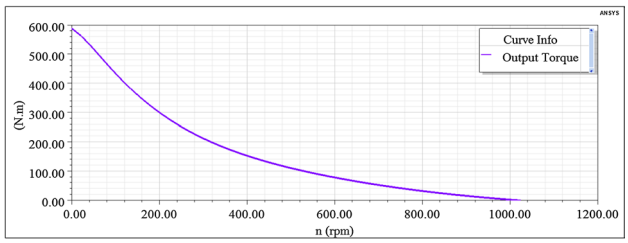

Fig. 9 Torque versus speed

The motor runs at the most effective range when it was at 830 rpm, as seen in Fig. 7.

Figure 8 shows the relationship between output power and speed. Depending on the motor speed, the output power value continued to increase and reached a peak value of 280–320 rpm. After this point, the output power value continued to decrease rapidly as the motor speed increased. This graph fits with the maximum output power and rated power values of the designed BLDC motor.

Figure 9 shows the relationship between torque and speed. The motor produced high starting torque to obtain a strong driving force during the initial moment. As the speed increased, the required torque decreased. As it seen in Fig. 9, the produced torque value was observed as around 23Nm when the motor reached its rated speed (830 rpm).

Figure 10 shows the relationship between torque-power, speed-power and efficiency-power. While the motor was drawing at 1.5 kW, the motor speed, the produced torque

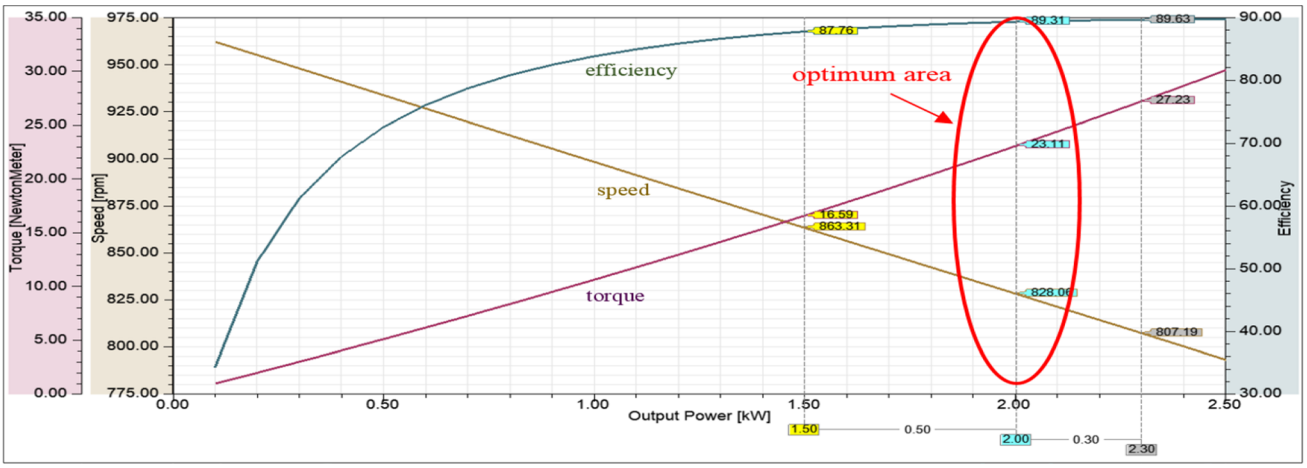

Fig. 10 Curves of 2 kW out-runner permanent magnet BLDC motor after optimization process

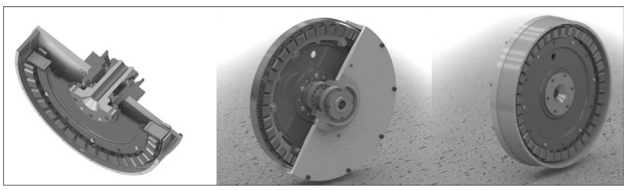

Fig. 11 3D visuals of the designed BLDC motor

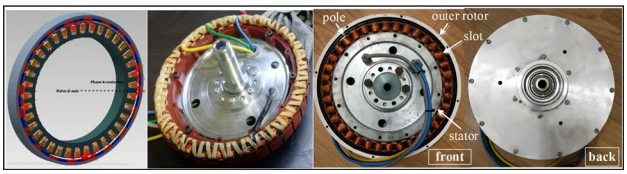

Fig. 12 Stator winding process

and the motor efficiency were at 863.31 rpm, 16.59 Nm and 87.76%, respectively. While the motor was drawing at 2 kW, the motor speed, the produced torque and the motor efficiency were at 828.06 rpm, 23.11 Nm and 89.31%, respectively. While the motor was drawing at 2.3 kW, the motor speed, the produced torque and the motor efficiency were at 807.19 rpm, 27.23Nm and 89.63%, respectively.

4 Prototype implementation

The motor has taken its final form after the analytical design and FEM-based validation and optimization processes. 3D visuals of the designed BLDC motor are shown in Fig. 11.

Stator winding process of the newly designed three-phase, 36 slot, 40 pole BLDC motor is shown in Fig. 12. 2 mm wire and 16 conductors in the groove were used for the stator winding. Phase–phase resistance was calculated as 140 mΩ. During the winding process, attention was paid to the correct placement of the coils and to the coil insulation to avoid short circuits. Figure 12 shows the stator winding process.

The BLDC motor was produced with ~ 10.4 kg. With an electromagnetic powder brake, the experimental loading

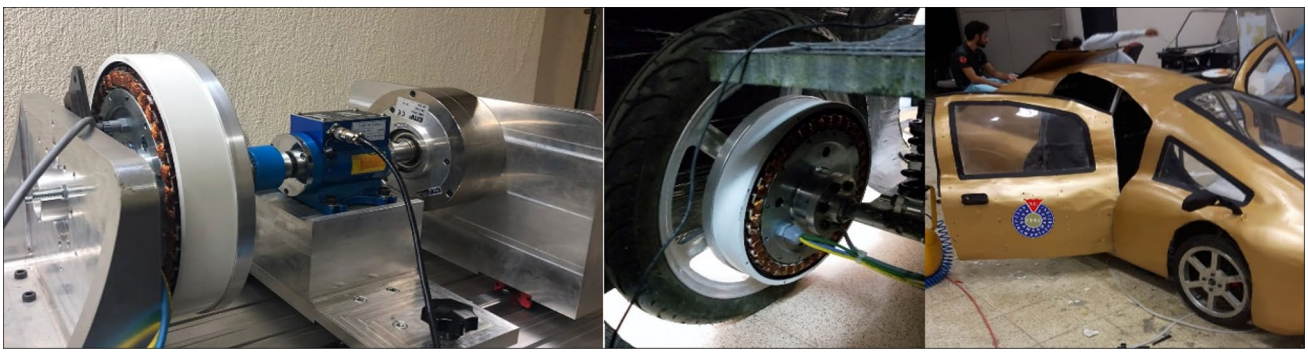

Fig. 13 Test and implementation works of BLDC motor

Table 7 Comparison of designed and experimental motor parameters

Parameters	Design	Experimental (loaded)
Rated power	2 kW	2 kW
Rated speed	828.06 rpm	815.16 rpm
Rated torque	23.11 Nm	21.4 Nm
Efficiency	89.31%	88.76%
Rated voltage	96 V	96 V
Stator material	M330-50A	M330-50A
Rotor material	AISI/SAE 4340 alloy steel	AISI/SAE 4340 alloy steel
Magnet type	N40UH	N40UH

process was performed manually. The test and implementation works of BLDC motor are shown in Fig. 13.

The produced BLDC motor was loaded until it consumes 2 kW shaft power. Comparisons of designed and experimental BLDC motor parameters are given in Table 7.

This motor was mounted in-rear-wheel (left) of an EV weighing roughly 200 kg with the driver (pilot). The descriptive statistical values for designed BLDC motor are shown in Table 8.

5 Hybrid metaheuristic based speed estimations

Heuristic algorithms have been developed inspired by the structures of nature, in order to realize some purpose or solve the existing problem. With the convergence function, they can produce a solution close to the exact solution. Compared to heuristic algorithms, metaheuristic algorithms are at the highest level thanks to their ability to minimize computational complexity, their success in nonlinear problems, their ability to memorize previous observations in local searches, and in a limited time to achieve effective results [26–29]. The hybrid model is formed by the integration of more than a variety of algorithms with appropriate characteristics. The aim of this model is to minimize the potential for error, to obtain better performance and more precise results from the performance of each component that constitutes it [30, 31].

In this study, to make the closest estimation and improve the system stability, a new hybrid model consisting of two distinctive metaheuristic algorithms, PSO and RMO, was used.

5.1 PSO

PSO, a metaheuristic algorithm, is a two-dimensional simulation of the behavior of birds and fish swarms together. It is a computationally efficient, effective and simple method in terms of implementation [32, 33]. In PSO, a bird or fish is expressed in terms of particles and the swarms are expressed in terms of the bird or fish population. In model, initial positions, velocities and population are randomly generated. By evaluating the initial values of each particle in the population, the suitability values are calculated. Gbest is the position value of the particle with the best value among the fitness values. Other particles according to this value update their position and velocity. The cycle continues until the termination step [33–36]. Parameters for PSO are given in Table 9 (Fig. 14).where c_1 is the effect of the best results the particle achieves on the next iteration, c_2 is the effect of the best results the swarm achieves on the next iteration, pbest is the position vector with local best values, gbest is the global position with the best value in each iteration defined by Eq. (22). X_i is the position vector, v_i is the velocity vector defined by Eq. (23). w is the inertia weight defined by Eq. (24) [32–34, 36]. Figure 15 shows motion of k particles.

5.2 RMO

RMO is a swarm-based, fast, simple and effective metaheuristic optimization technique designed for the global optimization of complex and nonlinear optimization problems. RMO has a less memory-requiring search method that can perform a faster and more intensive search around the target point. Particles require less memory and with each iteration, they move from an updated location.

Table 8 Descriptive statistical values for designed BLDC motor

Criteria	Efficiency	Output torque	Output power	Rated speed
Mean	0.677	54.544	2.641	775.404
Median	0.725	42.096	2.914	776.047
Standart deviation	0.153	46.032	1.427	151.532
Variance	0.023	2118.935	2.037	22,962.040
Maximum	0.791	164.942	4.328	1023.210
Minumum	0.000	0.000	0.000	517.444
Skewness	−2.700	0.802	−0.412	−0.017
Kurtosis	8.729	−0.370	−1.235	−1.217

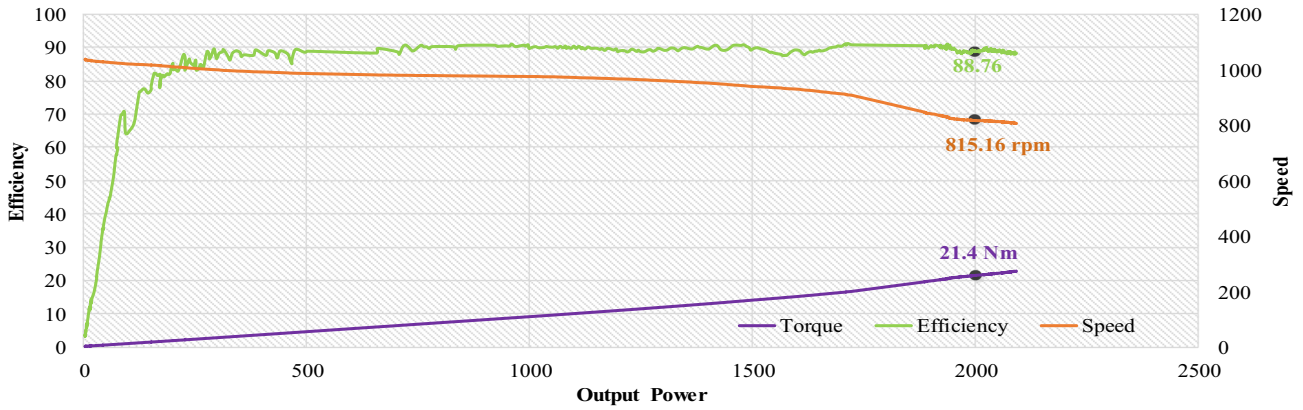

Fig. 14 Experimental curves of 2 kW out-runner permanent magnet BLDC motor (loaded)

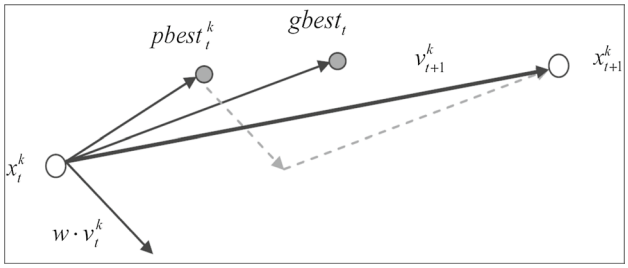

Fig. 15 Vector of the motion of k particles [37]

There is a best global vector in the update process that prevents the algorithm from being trapped at the local optimum [29, 38]. Parameters of RMO are given in Table 10.

where rand (0,1) can be derived from the normal distribution function between 0 and 1 as Gaussian distribution defined by Eq. (25), W is the inertia weight defined by Eq. (26), $V_{i,j}^k$ is the velocity vector of particle i in k. iteration defined by Eq. (27), c_p is the central point, up is the updating vector defined by Eq. (28), Rbest is the radial particle containing the best fitness value defined by Eq. (29) [27, 29, 38, 39]. Figure 16 shows the update *cp* vector via *up* vector (Fig. 17).

5.3 Hybrid metaheuristic (ANNs trained with PSO + RMO) model

By taking advantage of the distinctive individual features of PSO and RMO, this model is structured to be able to achieve

Table 9 Parameters of PSO

Prmtr	Definition	Description	Equations
V_i^k	$v_i^{k+1} = v_i^k + c_1 \cdot \text{rand}_1^k\left(\text{pbest}_i^k - x_i^k\right) + c_2 \cdot \text{rand}_2^k\left(\text{gbest}^k - x_i^k\right)$	Velocity vector of particle i in k. iteration	(22)
X_i^k	$x_i^{k+1} = x_i^k + v_i^{k+1}$	Position vector of particle i in k. iteration	(23)
v_{id}	$v_{\text{id}} = w \cdot v_{\text{id}} + \sum_{j \in N_i} \frac{c.r_j.(p_{jd} - x_{id})}{\lvert N_i \rvert}$	Velocity update of particle i	(24)

Table 10 Parameters of RMO

Prmtrr	Definition	Description	Equations
X_{ij}	$X_{ij} = X_{\min(j)} + \text{rand}(0,1) \cdot (X_{\max(j)} - X_{\min(j)})$	Position of particles	(25)
W_k	$W_k = W_{\max} - \left(\frac{W_{\max} - W_{\min}}{\text{Generation}_{\max}}\right) \cdot \text{Generation}_k$	Inertia weight	(26)
$V_{i,j}^k$	$V_{i,j}^k = W_k \cdot \text{rand}(0,1) \cdot V_{\max(j)}$	Velocity vector of particle i in k. iteration	(27)
c_p	${c_p}^{k+1} = {c_p}^k + \text{up}$	Central point	(28)
Up	$\text{up} = C_1 \cdot \left(\text{Gbest} - {c_p}^k\right) + C_2 \cdot (\text{Rbest} - {c_p}^k)$	Updating vector	(29)

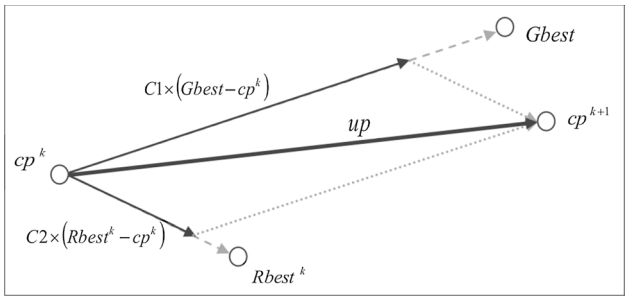

Fig. 16 Update the *cp* vector via vector *up* [38]

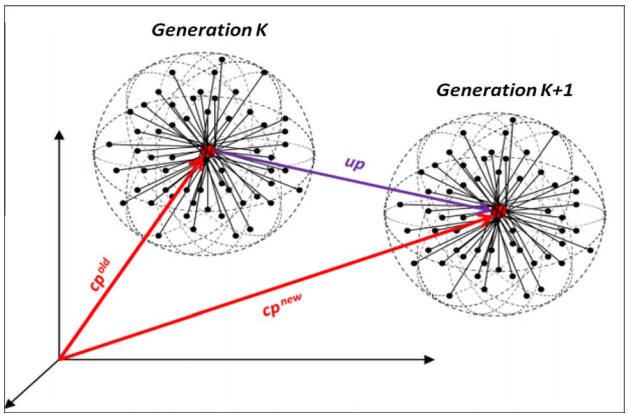

Fig. 17 Update *cp* via vector *up* [38]

such two unique characteristics of a single algorithm and increasing system efficiency. In this model, ANNs are used for estimation process, and then, ANNs are trained using PSO + RMO model. In the training process, it was aimed to optimize the linear–nonlinear components and random large fluctuations in the data sets. In MATLAB code, the data set was divided into three data sets: 70% training, 15% verification and 15% test data. The pseudocode of the ANNs trained with PSO + RMO model is shown in Fig. 18.

The process begins with the initialization of the weight parameters of the neural network. Then, it continues with the application of constraints and boundaries, evaluating the locations of all particles and keeping the best values. At generation control phase, if the number of production is an even, the RMO model becomes active, vice versa the PSO model becomes active, and then, the particles are sprinkled. The location matrix-weight parameters of the neural network are updated throughout that process and the stopping criteria are reviewed. If the criteria are not satisfactory, the process returns to the section "evaluate the locations of all particles and keep the best", and if sufficient, the process ends with the best values.

In this study, motor speed estimation was performed using ANNs trained PSO + RMO model. Its performance

```
Develop solution space by setting parameter space used in the algorithms
Set parameters of RMO W,C1,C2,C3
FOR every sample in population
        FOR every dimension in a sample
                X0 <- Initialize corresponding sample dimension as the
                difference of upper boundary and lower boundary
                multiplied with a random number in space 0 and 1
        END FOR
END FOR
Set initial population as X0
Set velocity vector as 0.7 times X0

FOR every sample in population
        F0 <- Evaluate initialized samples
END FOR
Store minimum value and index of Initialized samples F0
Set PBEST as X0 and GBEST as the minimum valued sample of X0 obtained
from F0 in the previous step
Initialize RMO with parameters and store Xi and CENTRE values
FOR every sample in population
        F1 <- Evaluate samples obtained as Xi
END FOR
Store minimum value and index of evaluated samples F1
Set best index as RBESTLOC of minimum value and best sample as RBEST
obtained from the minimum value of F1 through Xi
Set GBESTLOC as RBESTLOC and GBEST as RBEST
Set Iteration count and tolerance to 1
WHILE Iteration count and tolerance criterias are not met
        IF Iteration count is even
                Run RMO algortithm with calculated parameters
                FOR every sample in population
                        Evaluate sample and store in fitness matrix
                        Find the best sample through this matrix and
                        update GBEST iteration vector and
                        GBESTLOC vector
                END FOR
        ELSE iteration count is odd
                Repeat same procedure for PSO algorithm in the above
IF-END IF code clock
        END IF
Show best generation of the iteration
Update iteration count by adding one
END WHILE
```

Fig. 18 The pseudocode of the ANNs trained with PSO + RMO model

Fig. 19 Speed estimation procedure

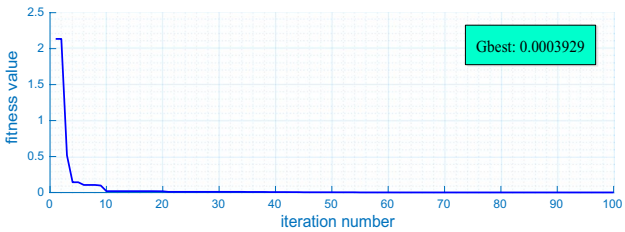

Fig. 20 Fitness value of ANNs trained with PSO + RMO model

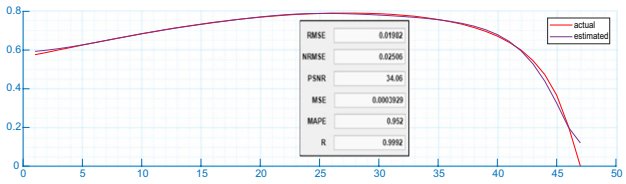

Fig. 21 The best actual and estimated curves of ANNs trained with PSO + RMO model

Table 11 Test error (MAPE,50run) comparison of hybrid models

Hybrid models	Test error (MAPE,50run)			
	Best	Average	Worst	SD
ANNs trained with PSO + RMO	0.952	2.728	4.807	1.063
ANNs trained with PSO	1.300	4.883	11.820	2.727
ANNs trained with GA	11.510	37.616	50.795	9.298
ANNs trained with ACO	19.729	39.298	53.690	7.781

ACO, Ant colony optimization; ANNs, Artificial neural networks; GA, Genetic algorithm; PSO, Particle swarm optimization; RMO, Radial movement optimization

in scenario-based wind speed and wind power prediction is the most major factor for considering this model [40, 41]. To evaluate the model's performance, a genuine and unconventional approach was used. That is, the output variable of motor speed is estimated using three distinct input variables such as output torque, efficiency and output power. Speed estimation procedure is shown in Fig. 19.

Fitness value and the best actual and estimated curves of ANNs trained with PSO + RMO model are shown in Figs. 20 and 21, respectively.

As shown in Fig. 21, the ANNs trained with PSO + RMO hybrid model resulted in estimating the motor speed estimation with a minimum error (MAPE: 0.952). Actual and estimated curves seem to be almost overlapping that it proves the success of the hybrid model.

Three distinct hybrid models (ANNs trained with PSO, ANNs trained with GA and ANNs trained with ACO) have been developed to compare the success of ANNs trained PSO + RMO model. Each hybrid model has been applied to the same data set and the results have been recorded in Tables 11 and 12.

Test error (MAPE,50run) comparison of hybrid models is shown in Table 11. This table was created by running each hybrid model 50 times. When the table is checked, it is obviously shown that ANNs trained with PSO + RMO model are by far the most successful technique with lowest errors.

The best test errors of hybrid models (ANNs trained with PSO + RMO, ANNs trained with PSO, ANNs trained with GA, ANNs trained with ACO) with six different error calculation techniques, nRMSE, RMSE, MSE, MAPE, PSNR and R, are shown in in Table 12.

6 Conclusion

In this study, a three-phase 2 kW in-wheel out-runner permanent magnet BLDC motor was designed for using in ultralight EVs. The size of the motor, the magnetic equivalent circuit and the electrical equivalent circuit parameters were analytically determined. Motor main dimensions, mechanical parameters and electrical-magnetic parameters have been carefully selected for motor performance. It was seen that motor dimensions, length of air gap, winding configuration, type of magnetic material, magnet selection and slot-fractional selections strongly affect the motor performance. After optimization studies, a BLDC motor with ~ %89 efficiency was achieved analytically. The FEM method was then used to approve of analytical design, and assess of flux density, flux distributions, torque and motor performance.

After analytical design and FEM confirmation, the prototype of the BLDC motor was produced. Motor performance under loads was recorded and analyzed. It was found 88.76% efficiency under load. As there was no significant difference between the modeling results and prototype results, thus, they confirmed each other (see Table 7). Then, the designed BLDC motor was mounted in-rear-wheel (left) of an ultralight EV.

Finally, by using a new robust hybrid metaheuristic called ANNs trained with PSO + RMO model, the motor speed was estimated. To observe the success of the model, despite the limited information given, it was desired to estimate the motor speed accurately. It mean using three distinct input variables such as output torque, efficiency and output power, the output variable of motor speed was estimated.

Table 12 The best test errors of hybrid models

Hybrid models	Best test errors					
	nRMSE	RMSE	MSE	MAPE	PSNR	*R*
ANNs trained with PSO + RMO	0.02506	0.01982	0.00039	0.9520	34.0600	0.9992
ANNs trained with PSO	0.02425	0.01918	0.00037	1.3000	34.3400	0.9992
ANNs trained with GA	0.11554	0.08862	0.00785	11.5100	21.0496	0.9788
ANNs trained with ACO	0.18856	0.14463	0.02092	19.7291	16.79500	0.9435

And then, three other hybrid metaheuristics, ANNs trained with PSO, ANNs trained with GA and ANNs trained with ACO, were designed for comparison it's performance. The test error comparisons of hybrid models, average MAPE values with 50 run, ANNs trained with PSO + RMO, ANNs trained with PSO, ANNs trained with GA and ANNs trained with ACO models are 2.728, 4.883, 37.616, 39.298, respectively (see Table 9). The best test errors of hybrid models including six different error calculation techniques such as nRMSE, RMSE, MSE, MAPE, PSNR and R are seen by far the success of ANNs trained with PSO + RMO model (see Table 12).

Acknowledgements This paper was presented to International Conference on Energy Systems, Drives and Automations (ESDA2020), Kolkata, India. It has been deemed worthy to receive The Best Paper Award. This work was funded by Scientific Research Projects Coordination Unit of Kahramanmaras Sutcu Imam University with project number: 2020/4-16M. And, the author thanks to Aegean Dynamics Corp. for all supports of prototyping process of the permanent magnet BLDC motor.

References

1. Kerem A (2014) Elektrikli araç teknolojisinin gelişimi ve gelecek beklentileri. Mehmet Akif Ersoy Üniversitesi Fen Bilimleri Enstitüsü Dergisi 5(1):1–13
2. Tumbek M, Kesler S (2019) Design and implementation of a low power outer-rotor line-start permanent-magnet synchronous motor for ultra-light electric vehicles. Energies 12(3174):1–20
3. Apatya YB, Subiantoro A, Yusivar F (2017) Design and prototyping of 3-phase BLDC motor. In: 15th International conference on quality in research (QiR): international symposium on electrical and computer engineering, Nusa Dua, pp 209–214
4. Shrivastava N, Brahmin A (2014) Design of 3-phase BLDC motor for electric vehicle application by using finite element. Int J Emerg Technol Adv Eng 4(1):140–145
5. Jurkovic M, Žarko D (2012) Optimized design of a brushless DC permanent magnet motor for propulsion of an ultra light aircraft. Automatika 53(3):244–254
6. Bogusz P, Korkosz M, Prokop J (2011) A study of design process of BLDC motor for aircraft hybrid drive. In: 2011 IEEE international symposium on industrial electronics, Gdansk, Poland
7. Castano SM, Maixé J (2012) Design of a brushless DC motor for an automotive application: a comparative evaluation with a commercial model. In: 2012 Workshop on engineering applications, Bogota, Columbia
8. Mukherjee P, Sengupta M (2014) Design, analysis and fabrication of a brush-less DC motor. In: 2014 IEEE international conference on power electronics, drives and energy systems (PEDES), Mumbai, India
9. Gholase V, Fernandes BG (2015) Design of efficient BLDC motor for dc operated mixer-grinder. In: 2015 IEEE international conference on industrial technology (ICIT), March 2015, Seville, Spain
10. Bogusz P, Korkosz M, Powrózek A, Prokop J, Wygonik P (2015) An analysis of properties of the BLDC motor for unmanned aerial vehicle hybrid drive. In: 2015 International conference on electrical drives and power electronics (EDPE), Tatranska Lomnica, Slovakia
11. Khergade A, Bodkhe SB, Rana AK (2016) Closed loop control of axial flux permanent magnet BLDC motor for electric vehicles. In: 2016 IEEE 6th international conference on power systems (ICPS), March 2016, New Delhi, India
12. He C, Wu T (2016) Design, analysis and experiment of a permanent magnet brushless DC motor for electric impact wrench. In: 2016 XXII international conference on electrical machines (ICEM), Sept. 2016, Lausanne, Switzerland
13. Jafarboland M, Farahabadi HB (2018) Optimum design of the stator parameters for noise and vibration reduction in BLDC motor. IET Electr Power Appl 12(9):1297–1305
14. Tutelea L, Boldea I (2007) Optimal design of residential brushless DC permanent magnet motors with fem validation. In: 2007 International Aegean conference on electrical machines and power electronics, Sept. 2007, Bodrum, Turkey
15. Nair SS, Nalakath S, Dhinagar SJ (2011) Design and analysis of axial flux permanent magnet BLDC motor for automotive applications. In: 2011 IEEE international electric machines and drives conference (IEMDC), May 2011, Niagara Falls, ON, Canada
16. Park Y, Kim H, Jang H, Ham S-H, Lee J, Jung D-H (2020) Efficiency improvement of permanent magnet BLDC with halbach magnet array for drone. IEEE Trans Appl Supercond 30(4):6523–6536
17. Shahri PK, Izadi V and Ghasemi AH (2020) Design a high efficiency and low ripple BLDC motor based on multi-objective optimization methods. In: 2020 American control conference Denver, July CO, USA
18. Singh VK, Marwaha S, Singh AK (2017) Design and analysis of permanent magnet brushless DC motor for solar vehicle using ANSYS software. Int J Eng Res Technol (IJERT) 6(4):1215–1220
19. Latha KL, Kumar MS (2016) Design topology and electromagnetic field analysis of permanent magnet brushless DC motor for electric scooter application. In: International conference on electrical, electronics, and optimization techniques (ICEEOT), March 2016, Chennai, India
20. Chang L, Muszynski J (2003) Design of a 5-phase permanent magnet brushless DC motor for automobiles. In: IEEE 58th vehicular technology conference. VTC 2003-Fall (IEEE Cat. No.03CH37484), Oct. 2003, Orlando, FL, USA
21. Devi KU, Sanavullah MY (2011) Performance analysis of exterior (outer) rotor permanent magnet brushless DC (ERPMBLDC) motor by finite element method. In: 3rd International conference on electronics computer Technology, April 2011, Kanyakumari, India
22. Umadevi N, Balaji M, Kamaraj V (2014) Design optimization of brushless DC motor using particle swarm optimization. In: IEEE 2nd international conference on electrical energy systems (ICEES), Chennai, India
23. Chasiotis ID, Karnavas YL (2018) A computer aided educational tool for design, modeling, and performance analysis of Brushless DC motor in post graduate degree courses. Comput Appl Eng Educ 26:749–767
24. Norhisam M, Nazifah A, Aris I, Wakiwaka H, Nirei M (2010) Effect of magnet size on torque characteristic of three phase permanent magnet brushless DC motor. In: Proceedings of 2010 IEEE student conference on research and development (SCOReD 2010), Putrajaya, Malaysia
25. Kumar A, Gandhi R, Wilson R, Roy R (2020) Analysis of permanent magnet BLDC motor design with different slot type. In: IEEE international conference on power electronics, smart grid and renewable energy (PESGRE2020), Jan. 2020, Cochin, India
26. Said GAENA, Mahmoud AM, El-Horbaty ESM (2014) A comparative study of meta-heuristic algorithms for solving quadratic assignment problem. Int J Adv Comput Sci Appl 5(1):1–6

27. Rahmani R, Rubiyah Y, Ismail N (2015) A new metaheuristic algorithm for global optimization over continuous search space. Int Conf Intell Comput 9:1335–1340
28. Karaboğa D (2011) Yapay zeka optimizasyon algoritmaları. Nobel Yayın Dağıtım, Ankara, pp 13–72
29. Mahrami M, Rahmani R, Seyedmahmoudian M, Mashayekhi R, Karimi H, Hosseini E (2016) A hybrid metaheuritic technique developed for hourly load forecasting. Complexity 21(1):521–532
30. Khashei M, Bijari M, Ardali GAR (2012) Hybridization of autoregressive integrated moving average (ARIMA) with probabilistic neural networks (PNNs). Comput Ind Eng 63(1):37–45
31. Ruiz-Aguilar JJ, Turias IJ, Jiménez-Come MJ (2014) Hybrid approaches based on SARIMA and artificial neural networks for inspection time series forecasting. Transp Res Part E Logist Transp Rev 67:1–13
32. Kennedy J and Eberhart R (1995) Particle swarm optimization. In: Proceedings of IEEE international conference on neural networks, Perth, Australia
33. Kennedy J, Eberhart RC, Shi Y (2001) Swarm intelligence. Morgan Kaufmann Publishers, San Francisco, p 512
34. Eberhart R, Kennedy J (1995) A new optimizer using particle swarm theory. In: Micro machine and human science proceedings of the sixth international symposium, Nagoya, Japan, October
35. Kennedy J and Eberhart RC (1997) A discrete binary version of the particle swarm algorithm. In: Proceedings of the conference on systems, man, and cybernetics, Orlando, FL, United States
36. Kennedy J, Mendes R (2006) Neighborhood topologies in fully informed and best-of-neighborhood particle swarms. Inst Electr Electron Eng Trans Syst Man Cybern Part C Appl Rev 36(4):515–519
37. Rahmani R, Yusof R, Seyedmahmoudian M, Mekhilef S (2013) Hybrid technique of ant colony and particle swarm optimization for short term wind energy forecasting. J Wind Eng Ind Aerodyn 123:163–170
38. Rahmani R, Yusof R (2014) A new simple, fast and efficient algorithm for global optimization over continuous search-space problems: radial movement optimization. Appl Math Comput 248:287–300
39. Seyedmahmoudian M, Horan B, Rahmani R, Maung Than Oo A, Stojcevski A (2016) Efficient photovoltaic system maximum power point tracking using a new technique. Energies 9(3):147
40. Kerem A, Saygin A (2019) Scenario-based wind speed estimation using a new hybrid metaheuristic model: particle swarm optimization and radial movement optimization. Meas Control 52(5–6):493–508
41. Kerem A, Saygin A, Rahmani R (2019) Wind power forecasting using a new and robust hybrid metaheuristic approach: a case study of multiple locations. In: 19th international symposium on electromagnetic fields in mechatronics, electrical and electronic engineering (ISEF), Aug. 2019, IEEE, Nancy, France